

# Loading, cooling and trapping of Strontium using intercombinaison line

T. Chanelière<sup>+</sup>, L. He<sup>\*</sup>, R. Kaiser and D. Wilkowski<sup>1</sup>

<sup>1</sup> Institut Non Linéaire de Nice, CNRS, UMR 6618,  
Université de Nice Sophia-Antipolis, F-06560 Valbonne, France.

<sup>+</sup> Now at: Laboratoire Aimé Cotton, CNRS, UPR 3321,  
Université Paris-Sud, Bat. 505, F-91405 Orsay Cedex, France

<sup>\*</sup> Now at: State Key Laboratory of Magnetic Resonance and  
Atomic and Molecular Wuhan Institute of Physics and Mathematics,  
Chinese Academy of Sciences, Wuhan 430071, P. R. China

(Dated: April 2, 2019)

The intercombinaison line of strontium at 689nm is successfully used in laser cooling to reach the photon recoil limit with Doppler cooling in a magneto-optical traps (MOT). In this paper we present a systematic study of the loading efficiency of such a MOT. Comparing the experimental results to a simple model allow us to discuss the actual limitation of our apparatus. We also study in detail the final MOT regime emphasizing the role of the gravity on the position, size and temperature along the vertical and horizontal directions. At large laser detuning, one finds an unusual situation where cooling and trapping occur in the presence of a high bias magnetic field.

PACS numbers: 39.25.+k

## I. INTRODUCTION

Cooling and trapping alkaline-earth atoms offer interesting alternatives to alkaline. Indeed, the singlet-triplet forbidden lines can be used for optical frequency measurement and related subjects [1]. Moreover, the spinless ground state of the most abundant bosonic isotopes leads, in principle, to more simple or at least different cold collisions problems than with alkaline atoms [2]. Considering fermionic isotopes, the long living and isolated nuclear spin can be controlled by optical means [3] and has been proposed to implement quantum logic gates [4]. It has been also showed that ultimate performance of Doppler cooling can be greatly improved by using narrow transitions. Whose photon recoil frequency shifts  $\omega_r$  are larger than their natural width  $\Gamma$  [5]. This is the case for the  $^1S_0 \rightarrow ^3P_1$  forbidden lines of Magnesium ( $\omega_r \approx 1100\Gamma$ ) or Calcium ( $\omega_r \approx 36\Gamma$ ). Unfortunately, both atomic species can not be hold in a standard magneto-optical trap (MOT) because the radiation pressure force is not strong enough to overcome the gravity. This imposes the use of an extra quenching laser as demonstrated for Ca [6]. For Strontium, the intercombinaison transition natural width ( $\Gamma = 2\pi \times 7.5$  kHz) is slightly broader than the frequency recoil shift ( $\omega_r = 2\pi \times 4.7$  kHz). The radiation pressure force is higher than the gravity and at the same time the final temperature is still in the  $\mu\text{K}$  range at the recoil limit[7, 8]. In parallel, the narrow transition partially prevents photon multiple scattering processes and the related atomic repulsive forces [9]. Then great improvements on the spatial density have been also reported [7]. Despite experimental efforts, this pure optical method has not allowed yet to reach quantum degeneracy regime.

In this paper, we will discuss performances, essentially the temperature and the loading rate, of a strontium 88 MOT on the 689 nm  $^1S_0 \rightarrow ^3P_1$  spin-forbidden line. First the atoms, initially in a MOT on the spin-allowed 461 nm  $^1S_0 \rightarrow ^1P_1$  transition as discussed in [10], are transferred into the 689 nm MOT. The laser spectrum is broadened by frequency modulation (FM) in order to increase the velocity capture range of the MOT. The results of this broadband cooling phase are presented in the section III. We discuss the intrinsic limitations of the loading efficiency. In our set-up, 50% of the atoms initially in the blue MOT are transferred in the red one, where the minimum temperature is about  $2.5\mu\text{K}$ . In order to reduce the temperature down to the photon recoil limit ( $0.5\mu\text{K}$ ), a second cooling phase is applied using a single line laser. In section IV, we describe the steady state MOT in this case. As already demonstrated the gravity plays a crucial role [11]. We more specifically compare the steady state behavior at large detuning along the  $z$  direction and in the  $x - y$  plane where gravity still affects the results.

## II. EXPERIMENTAL SET-UP

The MOT apparatus, on the broad  $^1S_0 \rightarrow ^1P_1$  transition at 461 nm, is described in references [12, 13]. Briefly, it is made of six independent laser beams with a typical intensity of  $10\text{ mW/cm}^2$ . The MOT magnetic field gradient is about  $70\text{ G/cm}$ . The blue MOT is fed by an atomic beam extracted from  $550^\circ\text{C}$  oven and longitudinally cooled by a Zeeman slower. With a flux of  $10^9$  atoms/s, the total number of atoms trapped in the blue MOT is about  $2.10^6$  within a  $0.6\text{ mm rms}$  radius cloud without any repumping lasers [14]. The typical temperature is  $10\text{ mK}$ , corresponding to a velocity dispersion of  $\sigma_b = 1\text{ m/s}$ . To optimize the transfer into the red MOT, the temperature of the blue MOT

should be as small as possible. As previously demonstrated [10], this temperature depends strongly on the optical field intensity. For this purpose, 4 ms before switching off the blue MOT, we decrease the intensity by a factor 5 (see figure 1). The rms velocity before the transfer stage is reduced down to  $\sigma_b = 0.6$  m/s whereas the rms size remains unchanged.

The 689 nm laser source is made by an anti-reflection coated laser diode mounted in a 10 cm long extended cavity. It is locked on an ULE cavity using the Pound-Drever-Hall technique [15]. The 20 MHz lateral bands necessary for the lock-in are obtained modulating the current of the laser diode. The unity gain of the servo loop is at a frequency of 1 MHz. From the noise spectrum of the error signal of the locking system, we derive a frequency noise power. It shows, in the range of interest, namely 1 Hz – 100 kHz, an upper limit of 160 Hz<sup>2</sup>/Hz which is low enough for our purpose. The transmitted light from the ULE cavity is injected into a 20 mW laser diode. Then noise components higher than the cavity frequency cut-off (300 kHz) and also the 20 MHz lateral bands are filtered. The long term drift of 10 – 50 Hz/s, mainly due to daily temperature change of the ULE cavity, are compensated with the help of a saturated spectroscopy set-up on the  $^1S_0 \rightarrow ^3P_1$  intercombinaison line.

The slave beam is sent through an acousto-optic modulator mounted in a double pass configuration. This acousto-optic modulator is used to switch on and off the red MOT beams. If required, namely during the loading phase (see section III), this acousto-optic modulator is also used for frequency modulation (FM) of the laser.

The red MOT is made of three retroreflected beams with a waist of 0.7 cm. The maximum intensity per beam is about 3 mW/cm<sup>2</sup> (the saturation intensity is  $I_s = 3 \mu\text{W}/\text{cm}^2$ ). The laser detuning can be tuned within the range of a few hundreds of linewidth around the resonance with the before mentioned acousto-optic modulator. Typical magnetic gradient used for the red MOT vary from 1 to 10 G/cm.

Once cooling and trapping with the intercombinaison line is achieved, a resonant 40  $\mu\text{s}$  pulse of blue light probes the cold cloud. The total fluorescence emitted during the pulse is collected on an avalanche detector. From this measurement, we deduce the number of atoms in the cloud and evaluate the transfer rate in the red MOT. At the same time, an image of the cloud is taken with an intensified CCD camera. The typical spatial resolution of the camera is 30  $\mu\text{m}$ . Varying the dark period between the red MOT phase and the blue probe, we get the ballistic expansion of the cloud. We then derive the velocity rms value and the corresponding temperature.

### III. BROADBAND LOADING OF THE RED MOT

The loading performances of a MOT depend strongly on the width of the transition. With a broad transition, the maximum radiation pressure force is typically  $a_m = \frac{v_r \Gamma}{2} \approx 10^4 \times g$ , where  $v_r$  is the recoil velocity. Hence, on a distance of  $l \approx 1$  cm, corresponding to a typical MOT beam waist, an atom with a velocity lower than  $v_c = \sqrt{2a_m l} \approx 30$  m/s can be captured. During the deceleration, the atom may be always close to resonance because the Doppler shift is in the same order than the linewidth. Thus MOTs can be loaded from a thermal vapor or from a slow atomic beam using single frequency lasers. Moreover typical magnetic field gradient of few tens of G/cm usually do not affect the resonance position and do not drastically change the loading.

An efficient loading is more complex to achieve with a narrow transition. For Strontium, the maximum radiation pressure force of a single laser is only  $a_m \approx 15 \times g$ . Assuming the radiation pressure force being maximum during all the capture process, one gets  $v_c = \sqrt{2a_m l} \approx 1.7$  m/s. Hence, precooling in the blue MOT greatly improves the loading rate. Moreover, the Doppler shift before deceleration is  $v_c \lambda^{-1} \approx 2.5$  MHz, thus 300 times larger than the linewidth. Hence, to keep the laser on resonance during the capture phase, the MOT lasers frequency should be broadened. Because of the low value of the saturation parameter, the laser spectrum can be large meanwhile the radiation pressure force remains maximal with a reasonable laser power. The magnetic field gradient of the MOT may also affect the velocity capture range. To illustrate this point, let's consider an atom initially in the blue MOT at the center of the trap with a velocity of  $v_c = 1.7$  m/s. During the deceleration, the Doppler shift decreases whereas the Zeeman shift increases. However, the magnetic field gradient may not affect the velocity capture, thus the loading, as far as the total frequency shift still decreases. This condition is fulfilled if the magnetic field gradient is lower than [16]:

$$b_c = \frac{a_m}{\lambda g \mu_b v_c} \approx 0.6 \text{ G/cm} \quad (1)$$

where  $g = 1.5$  is the Landé factor of the  $^3P_1$  level and  $\mu_b = 1.4$  MHz/G is the Bohr magneton.  $b_c$  is smaller than the magnetic field gradients used in the experiment. As we will see, it is usually necessary to increase the width of the laser spectrum such as the optimum transfer rate is not limited by the Zeeman shift (see section III B). An practical solution may consist of ramping the magnetic field gradient during the loading of the red MOT [7].

### A. Transfer rate: experimental results

In this section we will present experimental results concerning the loading efficiency of a red MOT form a blue one. To optimize the transfer rate, the laser spectrum is broaden using frequency modulation (FM). Thus the instantaneous laser detuning is  $\Delta(t) = \delta + \Delta\nu \sin \nu_m t$ .  $\Delta\nu$  and  $\nu_m$  correspond respectively to the frequency deviation and modulation frequency, where as  $\delta$  is the carrier detuning. Here, the modulation index  $\Delta\nu/\nu_m$  is always small and the narrowband limit is well fulfilled. Hence one can consider the FM spectrum has enclosed in the interval  $[-|\delta| - \Delta\nu; -|\delta| + \Delta\nu]$ .

As show in figure 2, the transfer rate increases with  $\nu_m$  up to 15 kHz where one observe a plateau at a transfer efficiency of 45%. Indeed, when  $\nu_m$  is larger than the linewidth, one are in the non-adiabatic regime and the atoms interact with all the fourier components of the laser spectrum. Moreover, the typical intensity per Fourier component remains always higher than  $I_s = 3 \mu\text{W/cm}^2$  the saturation intensity. As a consequence, the radiation pressure force should be close to its maximal value for any interacting atomic velocity. When  $\nu_m < \Gamma/2\pi$ , the atoms interact with a frequency chirped intense laser where the mean radiation pressure force (over a period  $2\pi/\nu_m$ ) is clearly smaller than in the  $\nu_m > \Gamma/2\pi$  regime. As a consequence, the transfer rate is reduced when  $\nu_m$  is decreased.

On figure 3, the transfer rate is plotted versus  $\Delta\nu$ . The carrier detuning is  $\delta = -1 \text{ MHz}$  and the modulation frequency, at  $\nu_m = 25 \text{ kHz}$ , is kept larger than the linewidth. Starting from no deviation ( $\Delta\nu = 0$ ), we observe an increase of the transfer rate with  $\Delta\nu$  (in the range  $0 < \Delta\nu < 500 \text{ kHz}$  for the parameters used in figure 3). After reaching its maximum value, the transfer rate do not depend on  $\Delta\nu$ . Thus the maximum initial velocity of trapped atoms, is not limited anymore by the laser spectrum. If the frequency deviation is still increasing, the transfer becomes again less efficient and rapidity decrease to zero. Because, the saturation parameter of each fourier component is larger than one, we can exclude that this decreasing is due to a reduction of the velocity capture range. On the other hand, if  $\Delta\nu > |\delta|$ , some components of the spectrum are blue detuned. This frequency configuration effects the performance of the MOT, and it is at the origin of the observed decreasing of the transfer rate. To confirm this interpretation, figure 4 shows the same experiment but with a larger detuning of  $\delta = -1.5 \text{ MHz}$  and  $\delta = -2 \text{ MHz}$  (figures 4a and 4b respectively). The transfer rate also starts to decrease when  $\Delta\nu > |\delta|$ . The transfer rate is also zero for small values of  $\Delta\nu$  because the carrier frequency is too red detuned. The radiation pressure forces are significant only for velocities larger than the capture velocity. Keeping now the deviation fixed and varying the detuning as shown in figure 5, we observe a maximum transfer rate when the detuning is close to the deviation frequency. Close to resonance, the blue detuned components prevent a good transfer rate.

We observe (figure 6) that the transfer rate decreases when the magnetic field gradient increases. At very low magnetic field ( $b < 1 \text{ G/cm}$ ) the reduction of the transfer rate is due to imperfections of the set-up such as non-balanced laser intensity, which induce a strong displacement of the cold cloud center of mass as observed experimentally. Hence, the optimum magnetic field gradient is fund to be the smallest one which ensure the stability of the cold atomic cloud in the MOT.

### B. Theoretical model and comparison with the experiments

To clearly understand the limiting processes of the transfer rate, experimental data are compared with a simple 1D theoretical model based on the following assumptions:

- An atom undergoes a radiation pressure force and thus a deceleration if the modulus of its velocity is between  $v_{max}$  and  $v_{min}$  with

$$v_{max} = \lambda(|\delta| + \Delta\nu), \quad v_{min} = \max\{\lambda(|\delta| - \Delta\nu); \lambda(-|\delta| + \Delta\nu)\} \quad (2)$$

Elsewhere  $a_m = 0$ . The condition  $v_{min} = \lambda(-|\delta| + \Delta\nu)$  is taken when some components are blue detuned. In this case, we consider the simple ideal situation where the two counter-propagating lasers are assumed perfectly balanced.

- Even in the semi-classical model, knowing the exact dependance in velocity of the acceleration, for the FM parameters, is a difficult task. However for all the data presented in this article, the saturation is larger than one. Hence the deceleration is set constant at  $-\frac{1}{3}a_m$  when  $v_{min} < |v| < v_{max}$ . The prefactor 1/3 takes into account the saturation of the transition by the counter-propagating laser beam pairs of the 3D configuration.

- The magnetic field gradient is included giving a spatial dependance of the detuning in the relations (2).

- An atom is considered to be trapped if its velocity changes sign within a distance shorter than the beam waist.

In figures 3-6 the results of the model are compared to the experimental data. The agreement between the model and the experimental data is good except at large frequency deviation (figures 3 and 4) or at low detuning (figure 5). In those cases the spectrum has some blue detuned components. It is a complex situation where the assumptions of the simple model do not hold anymore. Fortunately those cases do not have any practical interests because they do not correspond to optimum transfer efficiencies.

At maximum transfer rate, the model suggests that the transfer is limited by the beam waist (see caption of figures (3-6)). Moreover for all the situation explored in figures 3-5, the magnetic field gradient is strong enough ( $b = 1 \text{ G/cm}$ ) to have an impact on the capture dynamic, as suggested by the inequality (1). However it is not a limiting factor for the maximum transfer efficient because the Zeeman shift is compensated by a larger frequency excursion or by a larger detuning.

Increasing, the beam waist improves the transfer efficiency as showed on figure 7. If the saturation parameter remains high whatever the beam waist is, 90% of the atoms would be transferred for a 2 cm beam waist. In our experimental set-up, the power is limited to 3 mW per beam. So the saturation parameter is necessarily reduced once the waist is increased. To give a flavor of what one would expect, the previous acceleration is replaced by the expression  $a_{ms}/(1 + 3s)$ , with  $s = I/I_s$  the saturation parameter per beam. In this case, the transfer efficiency becomes maximum at 70% for a beam waist of 1.5 cm

### C. Temperature

Cooling with a broadband FM spectrum on the intercombiacion line decreases the temperature by three orders of magnitude with respect to the blue MOT from 3 mK ( $\sigma_b = 0.6 \text{ m/s}$ ) to  $2.5 \mu\text{K}$  (see figure 8). In this regime, the temperature is strongly increasing when the spectrum has some blue detuned components. Indeed the cooling force is reduced at the vicinity of zero velocity. This effect is illustrated by figure 8. At large detuning ( $\delta < -1.5 \text{ MHz}$ ), the temperature becomes constant. This regime correspond to a detuning independent steady state, similar to the one observed in single frequency cooling (see ref. [11] and section IV).

## IV. SINGLE FREQUENCY COOLING

About half of the atoms initially in the 461 nm MOT are recaptured in the red one using a broadband laser. The temperature is  $2.5 \mu\text{K}$  *i.e.* 5 times larger than the photon recoil temperature. To decrease further down the temperature one has to switch to single frequency cooling (for time sequences see figure 1). As we will see in this section, the minimum temperature is now around 600 nK close to  $0.8T_r$  the expected temperature in an 1D molasses [5].  $T_r = 460 \text{ nK}$  is the photon recoil temperature.

In the steady state regime of the red MOT, one has  $k\sigma_v \approx \omega_r \approx \Gamma$ . Thus, no separation of time scales exist such as in MOTs operated with a broad transition where  $\omega_r \ll k\sigma_v \ll \Gamma$ . Nevertheless, because of the high saturation regime, one has  $k\sigma_v \ll \Gamma\sqrt{1+s_T}$  and the semi-classical Doppler theory seems to correctly described most of the encountered experimental cases.  $s_T$  is the total saturation parameter taking into account all the MOT laser beams.

To insure an efficient trapping, the parameter range of the single frequency red MOT is different from a standard broad transition MOT; the magnetic field gradient is higher, typically  $1000 \text{ G/cm}$  and the MOT laser intensity is larger than the saturation intensity. Moreover the gravity is not negligible anymore with respect to typical laser radiation pressure forces. Those specificities lead to unusual behavior of the red MOT as we will try to explain in this section analyzing the MOT properties along the vertical dimension and in the horizontal plane.

### A. Vertical direction

The vertical temperature dependance as a function of the detuning of the red MOT is different from a broad transition MOT. Indeed, at large negative detuning (see examples on figure 9a), the temperature is constant. As explained in reference [11], this behavior can be understood noticing that the atom's dynamics is governed by competition between the gravity and the radiation pressure force of the upward laser. At large negative detuning, the downward laser is too detuned to give a significant contribution. In the semi-classical regime, an atom undergoes a net force of

$$F_z = \hbar k \frac{\Gamma}{2} \frac{s}{1 + s_T + 4(\delta - g_e \mu_B b z - k v_z)^2 / \Gamma^2} - mg \quad (3)$$

Considering initially the velocity dependance of the force, the first order term is:

$$F_z \approx -\gamma_z v_z \quad (4)$$

with

$$\gamma_z = -4 \frac{\hbar k^2 \delta_{\text{eff}}}{\Gamma} \frac{s}{\left(1 + s_T + 4\delta_{\text{eff}}^2/\Gamma^2\right)^2}$$

where the effective detuning  $\delta_{\text{eff}} = \delta - g_e \mu_B b < z >$  is defined such as

$$\hbar k \frac{\Gamma}{2} \frac{s}{1 + s_T + 4\delta_{\text{eff}}^2/\Gamma^2} = mg \quad (5)$$

Hence  $\delta_{\text{eff}}$  is independent of the laser detuning  $\delta$ .  $< z >$  is the mean vertical position of the cold cloud. Hence the vertical temperature at larger detuning depends only on the laser intensity and not on the laser detuning as it is showed in figures 9a and 9b.

Spatial properties of the cold cloud are also related to the fact that the effective detuning  $\delta_{\text{eff}}$  is independent of  $\delta$ . One has a linear dependence of mean vertical position of the cold cloud as function of the detuning such as

$$\frac{d < z >}{d|\delta|} = \frac{-1}{g_e \mu_B b} \quad (6)$$

Thus predicted vertical displacement can be compared to the experimental data in figure 10a. The agreement is excellent as the only adjustable parameter is the unknown origin of the vertical axis. Because the radiation pressure force for an atom at rest do not depend on the laser detuning  $\delta$ , it is also the case for the vertical rms size of the cold cloud. this point is also verified experimentally (see figure 10b).

### B. $x - y$ horizontal plane

Lets now study the behavior of the cold cloud in the  $x - y$  plane when the laser detuning is still large. The position of the cold cloud is vertically shifted downward with respect to the center of the magnetic field quadrupole (see figure 11). Thus we have to face to the unusual situation where cooling and trapping occur in the presence of a high bias magnetic field perpendicular to the cooling plane at the center of the cold cloud. For reasons of simplicity, we consider a spatially isotope magnetic field gradient  $b > 0$ . In the semi-classical limit, the expression of the radiation pressure force for each horizontal lasers counter-propagating pair has the form

$$F_x = \hbar k \frac{\Gamma}{2} \left( \frac{s(1 - \sin \alpha)^2/4}{1 + s_T + 4(\delta - g_e \mu_B b < z > (1 + |\tan \alpha|) - kv_x)^2/\Gamma^2} - \frac{s(1 + \sin \alpha)^2/4}{1 + s_T + 4(\delta - g_e \mu_B b < z > (1 + |\tan \alpha|) + kv_x)^2/\Gamma^2} \right) \quad (7)$$

$\alpha$  is the angle between the local magnetic field and the vertical axis (see figure 11b). For large detuning,  $\alpha$  is always a small quantity. The prefactor  $(1 \pm \sin \alpha)^2/4$  comes from the projection of circular polarization states of the horizontal lasers into the polarization eigenstate corresponding to the resonant transition. At  $\alpha = 0$ , *i.e.*  $x = 0$ , the polarization eigenstate corresponds exactly to the one coupled by the vertical upward laser. The other off-resonant transitions are rejected. One has to note that the Zeeman shift is the same for a pair of counter-propagating horizontal lasers. Moreover for an atom at equilibrium, the effective detuning  $\delta_{\text{eff}} = \delta - g_e \mu_B b < z >$  is obviously the same than the one found along the vertical dimension.

Linearizing with respect to  $\alpha$  and  $kv_x/\Gamma$  the expression 7 of the horizontal radiation pressure force, one gets:

$$F_z \approx -\kappa_\alpha \alpha - \gamma_x v_x = -\kappa_x x - \gamma_x v_x \quad (8)$$

with

$$\kappa_\alpha = < z > \kappa_x = \hbar k \frac{\Gamma}{2} \frac{s}{1 + s_T + 4\delta_{\text{eff}}^2/\Gamma^2} = mg$$

and

$$\gamma_x = \frac{\gamma_z}{2} = -2 \frac{\hbar k^2 \delta_{\text{eff}}}{\Gamma} \frac{s}{\left(1 + s_T + 4\delta_{\text{eff}}^2/\Gamma^2\right)^2}$$

Like for the vertical dimension, the expression of the cooling force does not depend on the laser detuning  $\delta$ . Hence, at large detuning, the horizontal temperature depends only on the intensity as observed in figures 9a and 9b.

To understand the trapping mechanisms in the  $x - y$  plane, let's consider an atom at rest at a position  $x \neq 0$  namely  $\alpha \neq 0$  like the one sketched in figure 11b. The transition rate of two counter-propagating laser beam is not anymore balanced due to the opposite sign in the  $\alpha$  dependance of the prefactor in expression 7. This mechanism leads to a restoring force in the  $x - y$  plane at the origin of the space confinement as expressed in equation 8. Applying the equipartition theorem one can connect the horizontal *rms* size of the cold cloud to the temperature by:

$$x_{\text{rms}}^2 = \frac{k_B T}{\kappa_x} = \frac{\langle z \rangle k_B T}{mg} \quad (9)$$

The agreement with experimental data is very good on the example showed on figure 10b. At the same time, the  $\delta$  dependency of the cloud displacement in the  $x - y$  plane is zero as long as the equilibrium of the counter-propagating beams intensities is preserved while the cloud moves in the vertical direction as it is observed on figure 10a.

### C. Comparing the temperatures along horizontal and vertical axes

We have seen in the sections IV A and IV B that the gravity has a dominant impact on cooling in a MOT operated on the intercombinaison line. We should therefore expect different behaviors along the vertical axe and in horizontal plane. It is the case for the spatial distribution (figures 10a and 10b) where as the temperatures are surprisingly the same (figures 9a and 9b). We will give now few arguments which may explain this point.

In the semi-classical approximation, the temperature is define as the ratio between the friction and the diffusion term:

$$k_B T_i = \frac{\gamma_i}{D_i^{\text{abs}} + D_i^{\text{spo}}} \quad \text{with } i = x, y, z \quad (10)$$

$D^{\text{abs}}$  and  $D^{\text{spo}}$  correspond to the diffusion coefficients induce by absorptions and spontaneous emissions events respectively. The friction coefficients has been already derived (see equation 8) and one has found:

$$\gamma_z = 2\gamma_{x,y} \quad (11)$$

Indeed cooling in the  $x - y$  plane results in the action of two counter-propagating beams four times less coupled than the upward laser. The same argument hold for the absorption term of the diffusion coefficient. Thus:

$$D_z^{\text{abs}} = 2D_{x,y}^{\text{abs}} \quad (12)$$

The contribution of spontaneous emissions in the diffusion coefficient can be derived form the differential cross-section  $d\sigma/d\Omega$  of the emitting atom [17]. With a strong biased magnetic field along the vertical direction, this calculation is particularly simple because the atom is excited only by a laser with a circular polarization state. Hence

$$d\sigma/d\Omega \propto (1 + \cos \phi^2) \quad (13)$$

$\phi$  is the angle between the vertical axe and the direction of observation. After a straightforward integration, one finds a contribution again two times larger along the vertical axe:

$$D_z^{\text{spo}} = 2D_{x,y}^{\text{spo}} \quad (14)$$

From those considerations, the temperature is expected to be isotropic as it is observed experimentally (see figures 9a and 9b).

For  $s \gg 1$ , the minimum temperature is given in the semi-classical Doppler cooling theory by the expression:

$$T = N_R \frac{\hbar \Gamma}{2k_B} \sqrt{s} \quad (15)$$

Where  $N_R$  is a numerical factor found to be close to two [11]. This solution is represented in figure 9 as a dash curve which match nicely the experimental data for  $s > 8$  but with  $N_R = 1.2$ . Similar results, *i.e.* with unexpected low  $N_R$  values, are found in [11]. For  $s \leq 8$  we observed a plateau in the final temperature close but still higher than the low saturation theoretical prediction [5]. We cannot explain why the temperature do not decrease further down as it is reported in [11]. For quantitative comparison with the theory, studies in a horizontal 1D molasses are in preparation [18].

#### D. Conclusions

Cooling of strontium atoms on the intercombinaison line is a efficient technique to reach the recoil temperature with optical means. However, the loading phase could not be done directly with a single frequency laser because of the narrow velocity capture range. We have shown that more than 50% of atoms initially in the blue MOT on the dipole-allowed transition are recaptured in the red MOT using a broad spectrum. The transfer rate depends on the parameters of the broadband cooling scheme. Using a simple model, we can conclude that the transfer is limited by the size of the laser beam. If the total power of the beams at 689 nm was not limited, transfer rates up to 90% would be expected by doubling our laser beam size. The final temperature in the broadband regime is found to be as low as  $2.5 \mu\text{K}$ , *i.e.* 5 times larger than the photon recoil temperature. The gain in temperature with respect to the blue MOT ( $1 - 10 \text{ mK}$ ) is appreciable. So, if no strong requirements in temperature is expected, broadband cooling is very efficient because it is reasonably fast (less than 100 ms) and the requirements for the laser frequency noise are less stringent than for single frequency cooling.

Using a single frequency cooling, after the broadband cooling, it is possible to reduce the temperature down to 600 nK slightly higher than the photon recoil temperature the 1D molasses prediction  $0.8T_r$ . The gravity is non negligible with respect to the semi-classical radiation pressure force and plays an important role in the steady state regime. In particular at large negative detuning, the cold cloud is shifted downwards into a region where the magnetic field gradient of the MOT induces a strong static field in the vertical dimension. Hence the laser detuning is compensated by a Zeeman shift so that the atoms *see* a constant detuning. As a consequence, the temperature becomes independent of the laser detuning and the spatial trapping in the  $x - y$  plane is due to atoms-laser coupling efficiency imbalance between counter-propagating waves.

#### V. ACKNOWLEDGMENTS

The authors wish to thank J.-C Bernard and J.-C. Bery for fruitfully technical support. This research is financially supported by the CNRS (Centre National de la Recherche Scientifique) and the former BNM (Bureau National de Métrologie) actually LNE (Laboratoire national de métrologie et d'essais) contract N° 03 3 005.

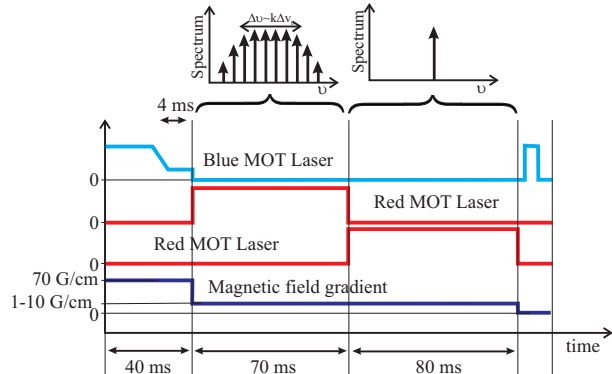


FIG. 1: Time scale and cooling phases of strontium on the intercombinaison line.

---

[1] F. Ruschewitz, J. L. Peng, H. Hinderth, N. Schaffrath, K. Sengstock, and W. Ertmer, *Phys. Rev. Lett.* **80**, 3173 (1998); G. Ferrari, P. Cancio, R. Drullinger, G. Giusfredi, N. Poli, M. Prevedelli, C. Toninelli, and G. M. Tino *Phys. Rev. Lett.* **91**, 243002 (2003); M. Yasuda and H. Katori *Phys. Rev. Lett.* **92**, 153004 (2004); T. Ido, T. H. Loftus, M. M. Boyd, A. D. Ludlow, K. W. Holman, and J. Ye *Phys. Rev. Lett.* **94**, 153001 (2005); R. Le Targat, X. Baillard, M. Fouch, A. Brusch, O. Tcherbakoff, G. D. Rovera, and P. Lemonde *Phys. Rev. Lett.* **97**, 130801 (2006).

[2] J. Weiner, V. Bagnato, S. Zilio, and P. S. Julienne, *Rev. Mod. Phys.* **71**, 1 (1999); T. Dinneen, K. R. Vogel, E. Arimondo, J. L. Hall, and A. Gallagher, *Phys. Rev. A* **59**, 1216 (1999). A.R.L.Caires, G.D.Telles, M.W.Mancini, L.G.Marcassa, V.S.Bagnato, D.Wilkowski, R. Kaiser, *Bra. J. Phys.* **34**, 1504 (2004).

[3] M. M. Boyd, T. Zelevinsky, A. D. Ludlow, S.M. Forman, T. Ido, and J. Ye *Science* **314**, 1430 (2006).

[4] D. Hayes, P. Julienne, I. Deutsch, Arxiv, quant-ph/0609111.

[5] Y. Castin, H. Wallis, and J. Dalibard, *J. Opt. Soc. Am. B*, **6**, 2046 (1989).

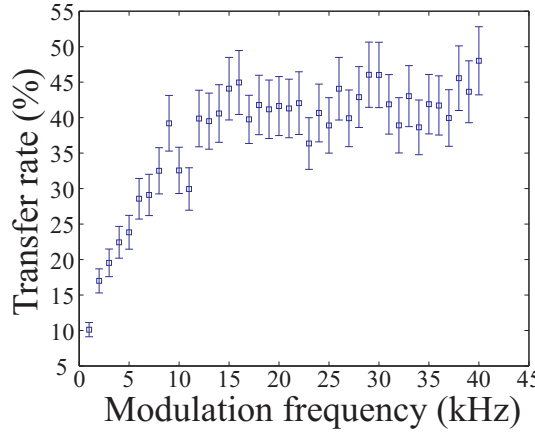


FIG. 2: Transfer rate as a function of the modulation frequency (squares). The other parameters are fixed:  $P = 3\text{ mW}$ ,  $\delta = -1000\text{ kHz}$ ,  $b = 1\text{ G/cm}$  and  $\Delta\nu = 1000\text{ kHz}$

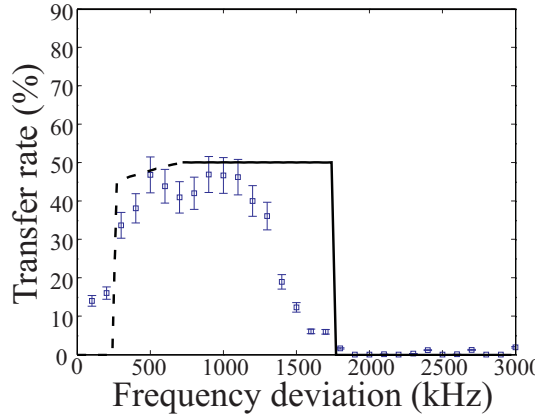


FIG. 3: Transfer rate as a function of the frequency deviation (squares). The other parameters are fixed:  $P$  is  $3\text{ mW}$   $\delta = -1000\text{ kHz}$ ,  $b = 1\text{ G/cm}$  and  $\omega_M = 25\text{ kHz}$ . The dash and solid line correspond to a simple model prediction (see text) where the limiting factors are the frequency deviation of the broad laser spectrum for the dash line and the waist of the MOT beam for the solid line.

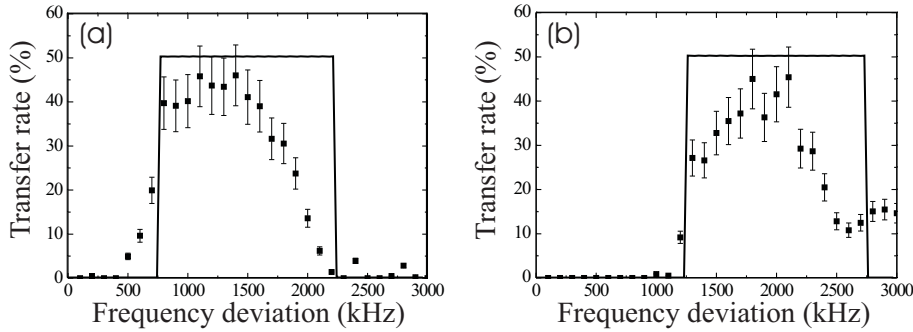


FIG. 4: Transfer rate as a function of the frequency deviation (squares).  $\delta = -1500\text{ kHz}$  and  $\delta = -2000\text{ kHz}$  for (a) and (b) respectively, the other parameters and the definitions are the same than for figure 3.

- [6] T. Binnewies, G. Wilpers, U. Sterr, F. Riehle, and J. Helmcke, T. E. Mehlstubler, E. M. Rasel, and W. Ertmer, Phys. Rev. Lett. **87**, 123002 (2001).
- [7] H. Katori, T. Ido, Y. Isoya, and M. Kuwata-Gonokami, Phys. Rev. Lett. **82**, 1116 (1999); T. H. Loftus, T. Ido, A. D. Ludlow, M. M. Boyd, and J. Ye, Phys. Rev. Lett. **93**, 073003 (2004).
- [8] T. Mukaiyama, H. Katori, T. Ido, Y. Li, and M. Kuwata-Gonokami Phys. Rev. Lett. **90**, 113002 (2003)
- [9] D. W. Sesko, T. G. Walker and C. E. Wieman, J. Opt. Soc. Am. B **8**, 946 (1991).

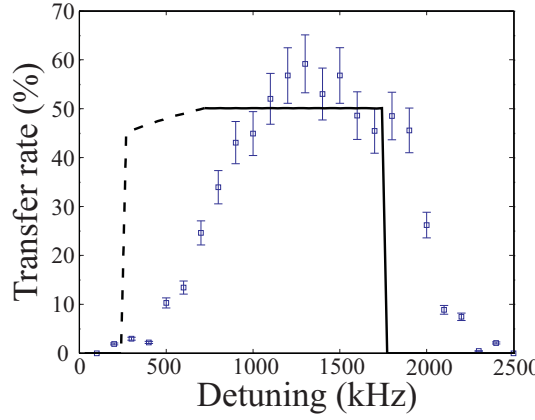


FIG. 5: Transfer rate as a function of the detuning (squares). The other parameters are fixed:  $P = 3\text{ mW}$ ,  $\Delta\nu = 1000\text{ kHz}$ ,  $b = 1\text{ G/cm}$  and  $\omega_M = 25\text{ kHz}$ . The dashed and solid lines have the same signification than in figure 3.

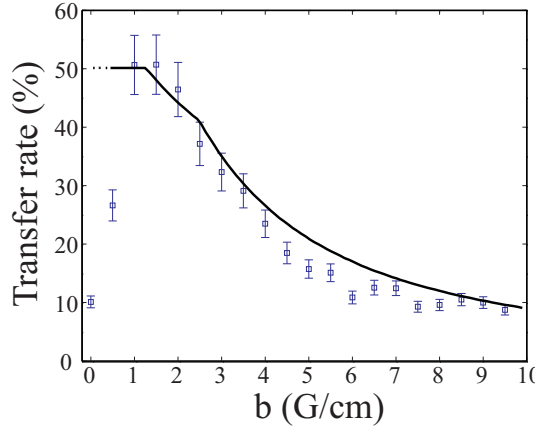


FIG. 6: Transfer rate as a function of the magnetic gradient (squares). The other parameters are fixed:  $P = 3\text{ mW}$ ,  $\delta = -1000\text{ kHz}$ ,  $\Delta\nu = 1000\text{ kHz}$  and  $\omega_M = 25\text{ kHz}$ . The limiting factor is the waist of the MOT beam for all values. The dotted lines represent the case where the magnetic field gradient do not affect the deceleration.

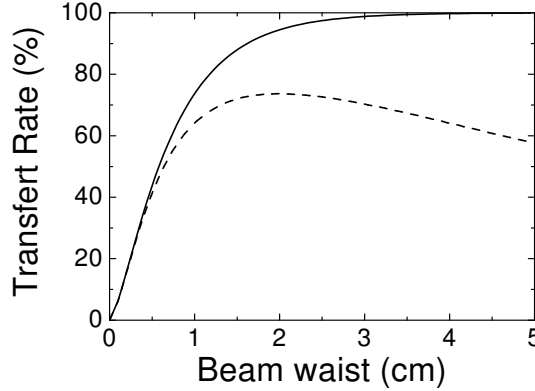


FIG. 7: Transfer rate as a function of the beam waist. The solid lines correspond to a high saturation parameter where as the dash line correspond to a constant power of  $P = 3\text{ mW}$ . The other parameters are fixed:  $\delta = -1000\text{ kHz}$ ,  $\Delta\nu = 1000\text{ kHz}$  and  $b = 0.1\text{ G/cm}$ .

- [10] T. Chanelière, J.-L. Meunier, R. Kaiser, C. Miniatura, and D. Wilkowski. *J. Opt. Soc. Am. B*, **22**, 1819 (2005).
- [11] T. H. Loftus, T. Ido, M. M. Boyd, A. D. Ludlow, and J. Ye, *Phys. Rev. A* **70**, 063413 (2004).
- [12] Y. Bidel, B. Klappauf, J.C. Bernard, D. Delande, G. Labeyrie, C. Miniatura, D. Wilkowski, R. Kaiser, *Phys. Rev. Lett.*

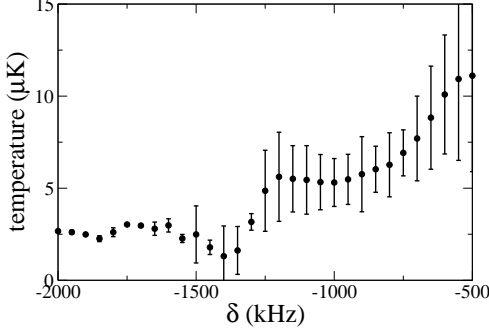


FIG. 8: Measured temperature as a function of the detuning for a FM spectrum. The other parameters are fixed:  $P = 3$  mW,  $b = 1$  G/cm,  $\Delta\nu = 1000$  kHz and  $\omega_M = 25$  kHz

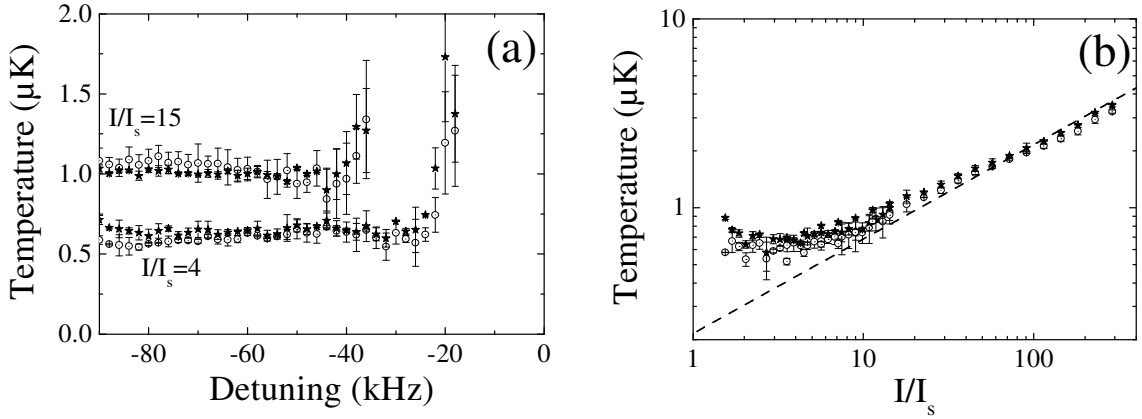


FIG. 9: Measured temperature as a function of the detuning (a) with  $I = 4I_s$  and as a function of the intensity (b) with  $\delta = -100$  kHz of single frequency cooling. The circles (respectively stars) correspond to temperature along one of the horizontal (respectively vertical) axis. The magnetic field gradient is  $b = 2.5$  G/cm

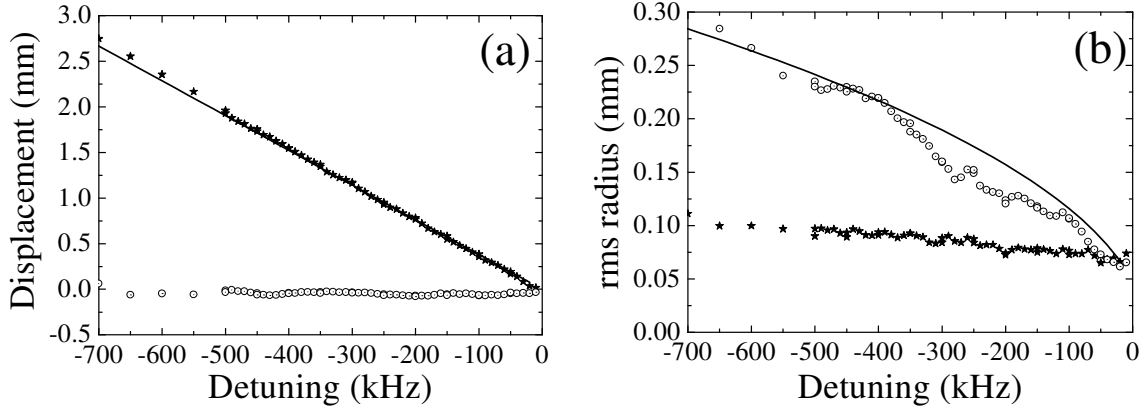


FIG. 10: Displacement (a) and rms radius (b) of the cold cloud in single frequency cooling along the  $z$  axis (star) and in the  $x - y$  plane (circle). The intensity per beam is  $I = 20I_s$  and the magnetic gradient  $b = 2.5$  G/cm along the strong axis in the  $x - y$  plane. The linear displacement prediction correspond to the plain line (graph a). The plain curve correspond to the rms radius prediction based on the equipartition theorem (graph b).

88, 203902 (2002).

[13] B. Klappauf, Y. Bidel, D. Wilkowski, T. Chanelière, R. Kaiser, Appl.Opt. **43**, 2510 (2004).

[14] D. Wilkowski, Y. Bidel, T. Chanelière, R. Kaiser, B. Klappauf, C. Miniatura, SPIE Proceeding **5866**, 298 (2005).

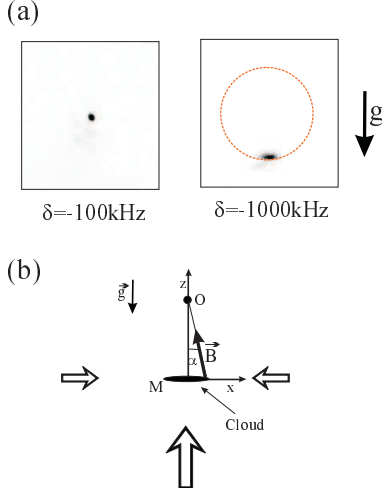


FIG. 11: (a) Images of the cold cloud in the red MOT. The cloud position for  $\delta = -100$  kHz coincides roughly with the center of the MOT whereas it is shifted downward for  $\delta = -1000$  kHz. The spatial position of the resonance correspond dot circle. (b) Sketch representing the large detuning case. The coupling efficiency of the MOT lasers is encoded in the size of the empty arrow. The laser form below has maximum efficiency whereas the one pointing downward is absent because is too detuned. Along a horizontal axe, the lasers are less coupled because they do not have the correct polarization. The  $\alpha$  angle is the angular position of an atom  $M$  with respect to  $O$ , the center of the MOT.

- [15] N. Poli, G. Ferrari, M. Prevedelli, F. Sorrentino, R. E. Drullinger, and G. M. Tino, *Spectro. Acta Part A* **63**, 981 (2006).
- [16] C. Dedman, J. Nes, T. Hanna, R. Dall, K. Baldwin, and A. Truscott, *Rev. Mod. Phys.*, **75**, 5136 (2004).
- [17] J.D. Jackson, *Classical Electrodynamics* (J. Wiley and sons, third edition New York, 1999).
- [18] D. Wilkowski et al. *in preparation*.